

## Brittle and ductile friction and the physics of tectonic tremor

Eric G. Daub,<sup>1,2</sup> David R. Shelly,<sup>3</sup> Robert A. Guyer,<sup>1,4</sup> and Paul A. Johnson<sup>1</sup>

Received 3 February 2011; revised 14 March 2011; accepted 27 March 2011; published 17 May 2011.

[1] Observations of nonvolcanic tremor provide a unique window into the mechanisms of deformation and failure in the lower crust. At increasing depths, rock deformation gradually transitions from brittle, where earthquakes occur, to ductile, with tremor occurring in the transitional region. The physics of deformation in the transition region remain poorly constrained, limiting our basic understanding of tremor and its relation to earthquakes. We combine field and laboratory observations with a physical friction model comprised of brittle and ductile components, and use the model to provide constraints on the friction and stress state in the lower crust. A phase diagram is constructed that characterizes under what conditions all faulting behaviors occur, including earthquakes, tremor, silent transient slip, and steady sliding. Our results show that tremor occurs over a range of ductile and brittle frictional strengths, and advances our understanding of the physical conditions at which tremor and earthquakes take place. **Citation:** Daub, E. G., D. R. Shelly, R. A. Guyer, and P. A. Johnson (2011), Brittle and ductile friction and the physics of tectonic tremor, *Geophys. Res. Lett.*, 38, L10301, doi:10.1029/2011GL046866.

### 1. Introduction

[2] The occurrence of earthquakes in the upper ~15 km of the crust indicates that the upper crust is generally brittle. With increasing depth and temperature, the mechanical properties gradually transition from brittle to ductile. Recent observations show that deformation in the brittle-ductile transition region often occurs transiently and is observed seismically as nonvolcanic tremor and low frequency earthquakes (LFEs) [e.g., *Obara, 2002; Rogers and Dragert, 2003; Shelly et al., 2006*], and geodetically as silent slip events [e.g., *Hirose et al., 1999; Dragert et al., 2001*]. Tremor and silent slip occur in many different tectonic regimes, and provide important clues into the nature of fault slip at depth.

[3] While many studies have examined the brittle-ductile transition in laboratory rock specimens [e.g., *Evans et al., 1990*], there are few observational constraints as to how this transition occurs in the earth. Modeling studies have focused on transient slip in the lower crust [e.g., *Liu and Rice, 2007; Ando et al., 2010*], but the physics that produces the slip behaviors observed at depth remains poorly understood. Figure 1a shows earthquake and tremor activity along the San Andreas Fault at Parkfield. Above ~15 km in the

seismogenic zone, rocks are brittle and earthquakes occur. Below ~15 km depth, the frictional properties change from brittle to ductile, where LFEs and tremor events occur.

[4] LFEs are located by identifying P and S wave arrivals on stacked seismic waveforms [*Shelly and Hardebeck, 2010*]. Additional occurrences of an event are identified by a cross correlation of the tremor waveforms with the seismic data at multiple 3-component stations at Parkfield [*Shelly et al., 2009*]. The set of repeated LFE occurrences at a single location are referred to as a “family,” and tremor is frequently concentrated in “bursts” where many events are observed in a short time window. The LFE bursts exhibit rich dynamics, including two period recurrence [*Shelly, 2010b*], complex migration along strike [*Shelly, 2010a*], and changes in activity associated with the 2004 Parkfield earthquake [*Shelly, 2009*].

[5] In this study, we develop a friction model for a single tremor family, and make comparisons with observed tremor dynamics. In particular, the observations provide two quantities associated with the tremor bursts: the recurrence time between successive bursts, and the duration of the bursts. Here, we focus on comparing the model to a tremor family with a shorter recurrence time of several days and duration of minutes, but the model can capture the dynamics of any tremor family. We utilize the basic observations to provide physical constraints on the nature of deformation at depth.

### 2. Brittle-Ductile Friction Model

[6] We approximate the slipping patch at depth corresponding to a single family as a block slider, as shown in Figure 1b. The block of mass  $m$  is attached to a spring with a stiffness per unit area of  $\Gamma$ , and the spring is pulled at a constant velocity  $V_0$ . The driving velocity  $V_0$  corresponds to the long-term slip rate on the San Andreas Fault, constrained through geodetic measurements to be about 30 mm/year [*Murray and Langbein, 2006*].

[7] The block motion is resisted by friction that is both brittle and ductile. The brittle friction is the sum over  $N_c$  frictional contacts [*Guyer, 2008*], which resist motion and fail suddenly, as illustrated in Figure 1c. These contacts represent regions smaller than the entire block, but larger than individual asperities, that can fail in a brittle manner. An idealized frictional contact forms at a position  $x_{0i}$  (left) and exerts a shear stress proportional to the displacement, with stiffness  $\gamma$  (center). When the displacement is larger than some failure distance  $a_i$ , the contact breaks and a new contact forms. When a contact breaks, the drop in friction causes the block to slip an amount that is dynamically determined by the equations of motion of the block and the dynamic evolution of the frictional contacts. The failure distances  $a_i$  are drawn from a probability distribution  $p_0(a) \propto a^{-2}$ , which reflects the roughness of the sliding interfaces. This distribution is consistent with laboratory experiments that measured asperity contact diameters of roughened surfaces [*Dieterich and*

<sup>1</sup>Geophysics Group, Los Alamos National Laboratory, Los Alamos, New Mexico, USA.

<sup>2</sup>Center for Nonlinear Studies, Los Alamos National Laboratory, Los Alamos, New Mexico, USA.

<sup>3</sup>U.S. Geological Survey, Menlo Park, California, USA.

<sup>4</sup>Physics Department, University of Nevada, Reno, Nevada, USA.

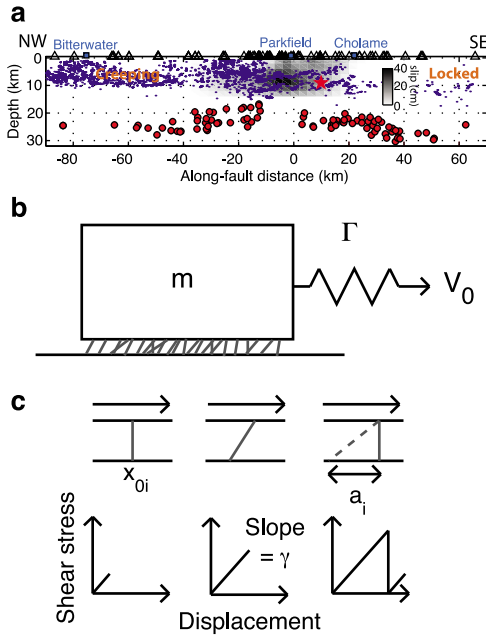


**Figure 1.** (a) Side view of the San Andreas Fault at Parkfield. At depths up to  $\sim 15$  km, fault slip occurs as earthquakes. Shading shows the fault slip in the 2004 Parkfield earthquake with the hypocenter indicated by the star, and the small dots indicate seismicity within 5 km of the fault [Waldhauser and Schaff, 2008]. At greater depths, tremor occurs, with the larger circles denoting LFE locations. Figure adapted from Shelly and Hardebeck [2010]. (b) Top view of the simple faulting model for tremor. Tremor at a single location is modeled as a rigid block pulled across a rough surface by a spring of stiffness  $\Gamma$  at a constant rate  $V_0$  [Murray and Langbein, 2006]. Friction is due to both brittle and ductile contacts between the block and the rough surface. (c) Failure of brittle contacts in the model. A contact forms at position  $x_{0i}$ , and as the surfaces slide it exerts a shear stress proportional to the displacement, with stiffness  $\gamma$ . When the contact reaches a specified failure length  $a_i$ , it breaks and renews with a new failure length drawn from the failure length distribution.

[Kilgore, 1996]. While this distribution is based on individual asperities, the evolution of the frictional strength of larger scale frictional interfaces occurs over a length scale similar to individual asperity diameters [Dieterich and Kilgore, 1994]. The model dynamics presented here are not dependent on the choice of  $p_0(a)$ , as simulations with  $p_0(a) = \text{const.}$  produce similar tremor behavior. The ductile friction damps the motion of the block. The ductile shear stress increases with the logarithm of velocity, consistent with laboratory friction experiments [Blanpied et al., 1995], with an overall strength  $\sigma_d$ .

[8] The equations of motion for the block are

$$\frac{m dV}{A dt} = \Gamma(V_0 t - x) - \sum_{i=1}^{N_c} \gamma(x - x_{0i}) - \sigma_d \log\left(\frac{V + V_0}{V_0}\right); \quad (1)$$

$$\frac{dx}{dt} = V. \quad (2)$$

Equation (1) is Newton's second law divided by the fault area  $A$  so that the frictional terms are expressed in terms of shear stress rather than force. The terms on the right hand side of equation (1) include the shear stress exerted by the spring, friction due to brittle contacts, and friction due to ductile contacts, respectively. Because friction is poorly constrained in the earth, we fix the other parameters and vary the brittle and ductile strengths. Additional model details and parameter choices are provided in the auxiliary material.<sup>1</sup>

### 3. Model Results

[9] Figure 2a shows the shear stress as a function of time. The block undergoes stick-slip motion, with stress drops of

<sup>1</sup>Auxiliary materials are available in the HTML. doi:10.1029/2011GL046866.

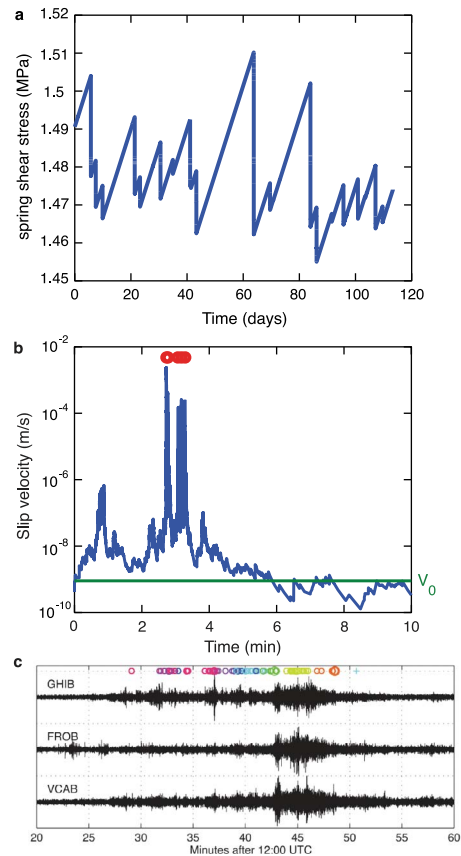


**Figure 2.** Plots of model LFE event dynamics for a brittle contact strength of 1 MPa and a ductile damping strength of  $\sigma_d = 0.007$  MPa. (a) Spring shear stress as a function of time. The block undergoes stick-slip motion. (b) Slip velocity as a function of time for a single stick-slip event. The horizontal line indicates the rate at which the spring is pulled. Each stick-slip event consists of several distinct failures, denoted by circles at the top of the plot. (c) Observations of LFEs at Parkfield. The plot shows seismic waveforms at three borehole stations. The circles at the top of the plot show when LFE events are detected, with different colors corresponding to LFEs at different spatial locations. During the burst of activity, there are multiple event occurrences within a short time period, as seen in the model. Figure taken from Shelly [2009].

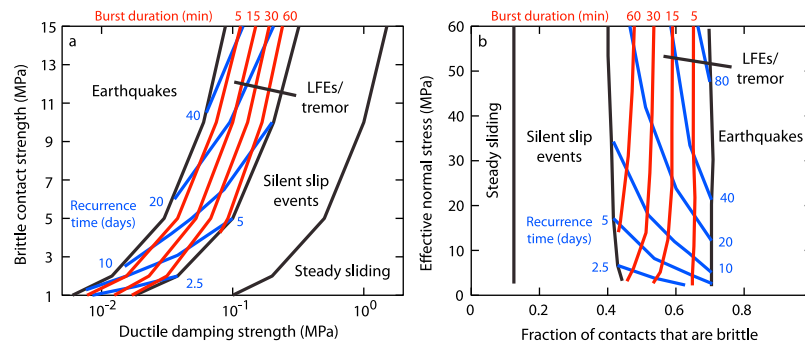


**Figure 3.** (a) Diagram illustrating the model dynamics as a function of the strength of the ductile damping term and the brittle contact strength. The model produces earthquakes for small values of the ductile term, and as the ductile strength increases, the model produces LFEs/tremor, silent slip, and steady sliding. At larger brittle strengths, a larger ductile damping strength is required for tremor to occur. Tremor observations can be characterized by the recurrence time between bursts and the duration of each burst. Within the range of model parameters that produce tremor, we show contours for recurrence time and burst duration to allow for comparisons to the observations. Details of how we differentiate between regions is described in the main text. (b) Diagram illustrating model dynamics, but with the axes transformed to indicate the fraction of contacts that are brittle on the horizontal axis, and effective normal stress on the vertical axis. Contours of recurrence time and burst duration are also shown. Tremor occurs over a range of the fraction of contacts that are brittle between 0.4–0.7, independent of the effective normal stress, though the contours show that the effective normal stress does have an effect on the recurrence time.

order 10 kPa. Figure 2b shows that each slip event consists of several discrete events. The model matches observations of bursts of LFEs at Parkfield. An example of LFE activity recorded by borehole seismometers at Parkfield is shown in Figure 2c. The colored circles indicate occurrence of various LFE families. Note that LFEs from a given family occur multiple times, as in the model. The uncertainties in tremor locations do not distinguish whether a burst of LFEs in a single family is due to several closely spaced patches failing successively, or a single patch failing repeatedly. Since the model is fairly simple, it does not distinguish between these possibilities either – each failure corresponds to a distinct collection of brittle contacts failing, though the entire block slips during each failure event. Bursts of activity are a common feature of tremor [Ide *et al.*, 2007], which indicates that our results are applicable to tremor in many tectonic settings.

[10] In the model, the recurrence time increases with increasing brittle contact strength, as the stress drop is larger. Recurrence time also increases as the ductile strength decreases, due to increased dynamic overshoot. Shorter burst durations occur for increased brittle strength, as the block slips more rapidly. Larger ductile damping strength leads to longer bursts by reducing the slip rate during failure.

[11] We perform a systematic study of the model dynamics as a function of the brittle and ductile strengths. Earthquake events have a single peak in the slip rate, rather than multiple peaks (tremor, Figure 2b). Steady sliding occurs when the slip rate is maintained within an order of magnitude of the driving rate  $V_0$ . Between these regimes, tremor occurs. Based on the seismic data, we estimate that tremor with a slip rate above  $10^{-4}$  m/s is detectable seismically (see auxiliary material). Therefore, events with a slip rate below  $10^{-4}$  m/s are silent slip events and are not detectable seismically, and events with a slip rate above  $10^{-4}$  m/s are LFEs/tremor that produce detectable seismic radiation.

[12] Figure 3a shows a phase diagram of the model dynamics as a function of the total brittle contact strength (the time average of the sum over all brittle contact stresses)

and the ductile damping strength  $\sigma_d$ . Tremor occurs over a range in the parameters. Within the tremor range, the model exhibits a variety of values for the recurrence time and burst duration. Contours show the recurrence time and burst duration produced by the model on the plot. For instance, a brittle strength of 1 MPa and a ductile damping strength of  $\sigma_d = 0.007$  MPa produces tremor bursts similar to observations of a family with recurrence of  $\sim 3$  days.

[13] Figure 3b shows the phase diagram in Figure 3a in terms of the effective normal stress and the fraction of contacts that are brittle. Contours again show recurrence time and burst duration within the range of parameters that produce tremor. We assume that the brittle friction has a friction coefficient of 0.7, and that the ductile damping is proportional to the normal stress by a factor of 0.01, based on laboratory experiments [Blanpied *et al.*, 1995]. LFEs occur if the fraction of contacts that are brittle is 0.4–0.7, independent of the effective normal stress. However, the effective normal stress does play a role in determining the recurrence time, as illustrated by the contours in Figure 3b. The model produces LFEs similar to the observed  $\sim 3$  day recurrence with a fraction of contacts that are brittle of 0.67 and a very low effective normal stress of 2.13 MPa. This suggests that the effective stress is low for families with short recurrence times. Higher values of the effective normal stress result in LFE families with longer recurrence times. Tremor at shallower depths tends to have longer recurrence times [Shelly, 2010a], suggesting that effective pressure is lower at large depths.

#### 4. Discussion

[14] The model shows that for observable tremor to occur, 40%–70% of the contacts must be brittle at depth. Laboratory studies show that quartz deforms in a ductile manner at a lower temperature than feldspar [Scholz, 1988], and exhumed strike-slip faults show evidence of brittle deformation of feldspar at the same depths as ductile deformation of quartz [Cole *et al.*, 2007]. Relative variations in the amount of

quartz and feldspar at different spatial locations at Parkfield [Solum *et al.*, 2006] could be responsible for the diverse tremor dynamics observed at Parkfield. At tremor depths of ~25 km at Parkfield, temperatures are ~600°C [Sass *et al.*, 1997]. Tullis and Yund [1992] showed that at low pressures, deformation of feldspar at 600°C can occur in a brittle manner. This suggests that low effective normal stress, which is needed to match observed recurrence times, may also be necessary for feldspar to remain brittle at large depths. The results also suggest that below the rupture segment of the 2004 Parkfield earthquake where no tremor has been observed (Figure 1a), ~40% or less of contacts are deforming in a brittle manner.

[15] Most models of the seismic cycle use the laboratory derived rate and state friction laws [e.g., Lapusta *et al.*, 2000] that do not explicitly include a combination of brittle and ductile processes. Deformation in the lower crust may precede earthquake nucleation in the seismogenic zone as suggested by changes in tremor migration patterns before the 2004 Parkfield Earthquake [Shelly, 2009]. Our model could provide additional clues as to how deformation in the lower crust is related to damaging earthquakes in the upper crust in many different tectonic settings.

[16] **Acknowledgments.** We thank Fred Pollitz and James Savage for helpful reviews. This work was supported by institutional support (LDRD) at Los Alamos.

[17] The Editor thanks Allan Rubin and an anonymous reviewer for their assistance in evaluating this paper.

## References

- Ando, R., R. Nakata, and T. Hori (2010), A slip pulse model with fault heterogeneity for low-frequency earthquakes and tremor along plate interfaces, *Geophys. Res. Lett.*, *37*, L10310, doi:10.1029/2010GL043056.
- Blanpied, M. L., D. A. Lockner, and J. D. Byerlee (1995), Frictional slip of granite at hydrothermal conditions, *J. Geophys. Res.*, *100*(B7), 13,045–13,064.
- Cole, J., B. Hacker, L. Ratschbacher, J. Dolan, G. Seward, E. Frost, and W. Frank (2007), Localized ductile shear below the seismogenic zone: Structural analysis of an exhumed strike-slip fault, Austrian Alps, *J. Geophys. Res.*, *112*, B12304, doi:10.1029/2007JB004975.
- Dieterich, J. H., and B. D. Kilgore (1994), Direct observation of frictional contacts: New insights for state-dependent properties, *Pure Appl. Geophys.*, *143*(1–3), 283–302.
- Dieterich, J. H., and B. D. Kilgore (1996), Imaging surface contacts: Power law contact distributions and contact stresses in quartz, calcite, glass and acrylic plastic, *Tectonophysics*, *256*(1–4), 219–239.
- Dragert, H., K. Wang, and T. S. James (2001), A silent slip event on the deeper Cascadia subduction interface, *Science*, *292*(5521), 1525–1528.
- Evans, B., J. T. Fredrich, and T.-F. Wong (1990), The brittle-ductile transition in rocks: Recent experimental and theoretical progress, in *The Brittle-Ductile Transition in Rocks*, *Geophys. Monogr. Ser.*, vol. 56, edited by A. G. Duba *et al.*, pp. 1–20, AGU, Washington, D. C.
- Guyer, R. A. (2008), Bristles, brooms, and butterflies, paper presented at the 13th Annual International Conference on Nonlinear Elastic Materials, Aix-en-Provence, France.
- Hirose, H., K. Hirahara, F. Kimata, N. Fujii, and S. Miyazaki (1999), A slow thrust slip event following the two 1996 Hyuganada earthquakes beneath the Bungo Channel, southwest Japan, *Geophys. Res. Lett.*, *26*(21), 3237–3240.
- Ide, S., G. C. Beroza, D. R. Shelly, and T. Uchide (2007), A scaling law for slow earthquakes, *Nature*, *447*, 76–79.
- Lapusta, N., J. R. Rice, Y. Ben-Zion, and G. Zheng (2000), Elastodynamic analysis for slow tectonic loading with spontaneous rupture episodes on faults with rate- and state-dependent friction, *J. Geophys. Res.*, *105*(B10), 23,765–23,789.
- Liu, Y., and J. R. Rice (2007), Spontaneous and triggered aseismic deformation transients in a subduction fault model, *J. Geophys. Res.*, *112*, B09404, doi:10.1029/2007JB004930.
- Murray, J., and J. Langbein (2006), Slip on the San Andreas Fault at Parkfield, California, over two earthquake cycles, and the implications for seismic hazard, *Bull. Seismol. Soc. Am.*, *96*(4B), S283–S303.
- Obara, K. (2002), Nonvolcanic deep tremor associated with subduction in southwest Japan, *Science*, *296*(5573), 1679–1681.
- Rogers, G., and H. Dragert (2003), Episodic tremor and slip on the Cascadia subduction zone: The chatter of silent slip, *Science*, *300*(5627), 1942–1943.
- Sass, J. H., C. F. Williams, A. H. Lachenbruch, S. P. Galanis Jr., and F. V. Grubb (1997), Thermal regime of the San Andreas fault near Parkfield, California, *J. Geophys. Res.*, *102*(B12), 27,575–27,585.
- Scholz, C. H. (1988), The brittle-plastic transition and the depth of seismic faulting, *Geol. Rundsch.*, *77*, 319–328.
- Shelly, D. R. (2009), Possible deep fault slip preceding the 2004 Parkfield earthquake, inferred from detailed observations of tectonic tremor, *Geophys. Res. Lett.*, *36*, L17318, doi:10.1029/2009GL039589.
- Shelly, D. R. (2010a), Migrating tremors illuminate complex deformation beneath the seismogenic San Andreas Fault, *Nature*, *463*, 648–652.
- Shelly, D. R. (2010b), Periodic, chaotic, and doubled earthquake recurrence intervals on the deep San Andreas Fault, *Science*, *328*(5984), 1385–1388.
- Shelly, D. R., and J. L. Hardebeck (2010), Precise tremor source locations and amplitude variations along the lower-crustal central San Andreas Fault, *Geophys. Res. Lett.*, *37*, L14301, doi:10.1029/2010GL043672.
- Shelly, D. R., G. C. Beroza, S. Ide, and S. Nakamura (2006), Low-frequency earthquakes in Shikoku, Japan and their relationship to episodic tremor and slip, *Nature*, *442*, 188–191.
- Shelly, D. R., W. L. Ellsworth, T. Ryberg, C. Haberland, G. S. Fuis, J. Murphy, R. M. Nadeau, and R. Bürgmann (2009), Precise location of San Andreas Fault tremors near Cholame, California using seismometer clusters: Slip on the deep extension of the fault?, *Geophys. Res. Lett.*, *36*, L01303, doi:10.1029/2008GL036367.
- Solum, J. G., S. H. Hickman, D. A. Lockner, D. E. Moore, B. A. van der Pluijm, A. M. Schleicher, and J. P. Evans (2006), Mineralogical characterization of protolith and fault rocks from the SAFOD Main Hole, *Geophys. Res. Lett.*, *33*, L21314, doi:10.1029/2006GL027285.
- Tullis, J., and R. Yund (1992), The brittle-ductile transition in feldspar aggregates: An experimental study, in *Fault Mechanics and Transport Properties of Rocks*, pp. 89–117, Academic, London.
- Waldhauser, F., and D. P. Schaff (2008), Large-scale relocation of two decades of Northern California seismicity using cross-correlation and double-difference methods, *J. Geophys. Res.*, *113*, B08311, doi:10.1029/2007JB005479.

E. G. Daub, R. A. Guyer, and P. A. Johnson, Geophysics Group, Los Alamos National Laboratory, MS D443, Los Alamos, NM 87545, USA. (edaub@lanl.gov)

D. R. Shelly, U.S. Geological Survey, 345 Middlefield Rd., Menlo Park, CA 94025, USA.